WHITE PAPER

Feasibility Study of a Fully-Digital Multi-Band SAR System operating at L, C, X and Ku Bands.

August 2022

CONTEXT

7th Workshop on RF and Microwave Systems, Instruments & Sub-systems + 5th Ka-band Workshop (10-12 May 2022).
Stefano Lischi[(1)], Riccardo Massini[(1)], Romain Pilard[(2)], Daniele Stagliano[(1)], Nicolas Chantier[(2)]
[(1)]ECHOES s.r.l. - Via M. Giuntini 63, 56023 Cascina - Italy
Email: stefano.lischi@echoes-tech.it, daniele.stagliano@echoes-tech.it, riccardo.massini@echoes-tech.it
[(2)]Teledyne e2v - Avenue de Rochepleine, 38126 Saint Egrève - France
Email: nicolas.chantier@teledyne.com

INTRODUCTION

Synthetic Aperture Radar (SAR) is an active imaging sensor employed in remote sensing applications that can achieve wide areas images in every weather condition. SAR imaging uses an antenna that is mounted on a moving platform. Through the processing of received echoes, SAR permits to obtain a larger synthetic antenna aperture which improves the azimuth resolution.

Radars at a specific frequency band usually have different capabilities, characteristics and applications than radars in other frequency bands. It is well known, for instance, that penetration capabilities essentially depend on microwave frequency [1]. Typically, penetration distance is inversely proportional to microwave frequency. The higher the frequency, the lower the penetration depth. Also, terrain characteristics affect penetration capabilities and humidity acts as a shield to microwave penetration [2]. Emerging military and civilian applications of P- and L-band radar systems include the detection of targets concealed by foliage and/or camouflage, detection of buried objects, forestry applications, biomass measuring, archaeological and geological exploration.

On the other hand, it is easier to obtain accurate range and position measurements at the higher radar frequencies, e.g., X-, Ku- and Ka-bands, since they have broader bandwidth (which determines range accuracy and range resolution) and narrower beam antennas for a given physical size antenna (which determines angle accuracy and angle resolution) [3]. From these considerations, it is clear the benefit that a single multi-band SAR system might produce in terms of operational flexibility and observation capabilities for different applications and end-users.

The purpose of this paper is to introduce the feasibility study of a multi-band SAR based on an emerging Teledyne e2v's proprietary Digital to Analogue Converter (DAC) and Analogue to Digital Converter (ADC) capable of direct signal generation and direct synthesis up to Ka-band. In particular, the direct signal generation can be done via a dual-channel DAC with wide instantaneous bandwidth (up to 6 GHz with 12 GSps) and a large output analogue bandwidth (up to 25 GHz). Such a feasibility study involves the analysis of key enabling technologies, the definition of a preliminary architecture and the preliminary design of a multi-band SAR system that can indeed be mounted onboard aerial platforms. Examples of components and expected performance in terms of Noise Equivalent Sigma Zero (NESZ), received power and data-rate are discussed.

KEY ENABLING TECHNOLOGIES: DAC AND ADC

Very high sampling frequency DAC and ADC with ultra-wide analogue bandwidth are the key enabling technologies for the proposed fully-digital multi-band SAR system.

In particular, the dual-channel EV12DD700 DAC [4] sampling at 12 GSps offers an instantaneous bandwidth of 6 GHz and it can operate simultaneously on multiple Nyquist Zones (NZ) up to a -3dB analogue bandwidth of 25 GHz. Multiple output modes including 2RF allow for an up-conversion-free direct signal synthesis at 21 GHz and beyond as illustrated in Fig. 1. Other features of the EV12DD700 DAC are: fast programmable complex mixer supporting highly agile frequency hopping; programmable anti-sinc filter; digital up-conversion and multi-device synchronization.

The EV12PS640 Proof-of-Concept ADC [5] is a single channel device with a chained synchronization feature for digital beamforming. Direct Radio Frequency (RF) sampling is supported up to 30 GHz with a single-ended ADC input as shown in Fig. 2. The single-ended input allows for the design of the receiver signal path without the use of RF balun and the associated signal distortion and bandwidth limitations. The sampling frequency up to 12.8 GSps provides a maximum width of NZ of 6.4 GHz.

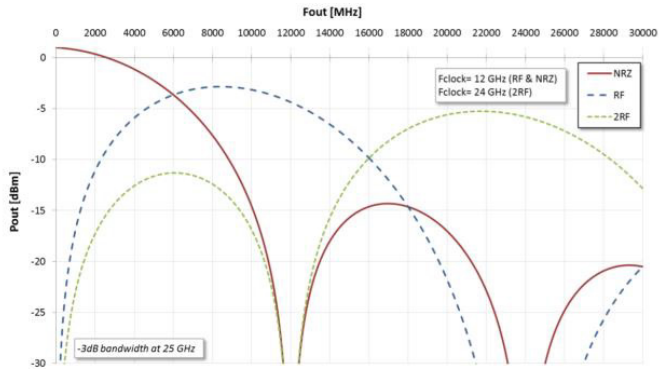

Fig. 1. DAC Output power vs Output frequency in various DAC operating modes.

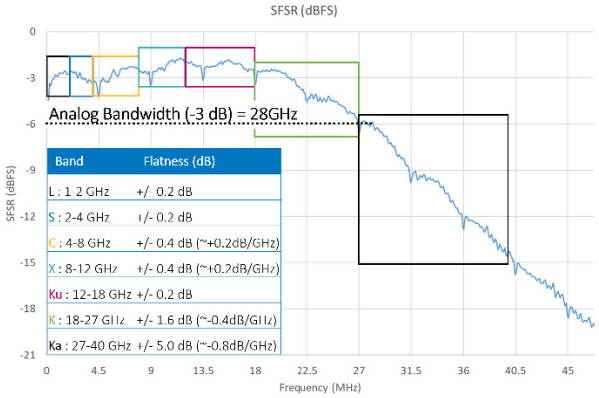

Fig. 2. Input bandwidth performance with single ended signals.

PRELIMINARY ARCHITECTURE

In this paper, a fully-digital four bands SAR is proposed. Thanks to the high sampling frequency up to 12 GSps, arbitrary L-band waveforms between 1÷1.5 GHz simultaneously with C-band signals in the 4.75÷5.5 GHz frequency range can be directly synthesized without overlap in the Non-Return-to-Zero (NRZ) mode. Also, since the DAC can operate in multiple NZs with the RF mode, X-band waveforms can be generated in the 2nd NZ simultaneously with the Ku-band pattern in the 3rd NZ. In particular, waveforms at 9÷10.2 GHz can be generated at X-band together with 16÷17.5 GHz at Ku-band. Fig. 3 shows the spectrum of noise-like waveforms at the DAC outputs.

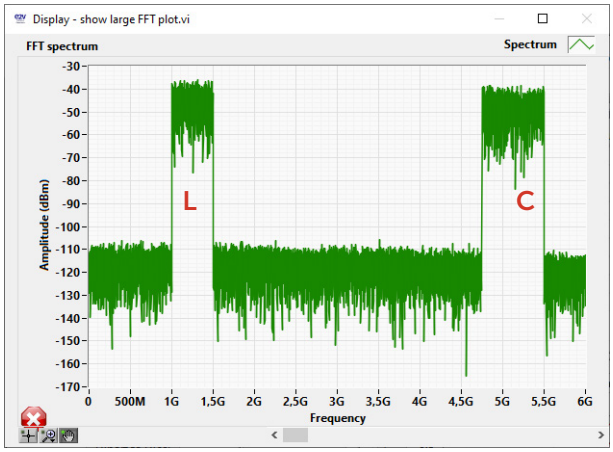

a) L+C band in NRZ mode in the 1st NZ.

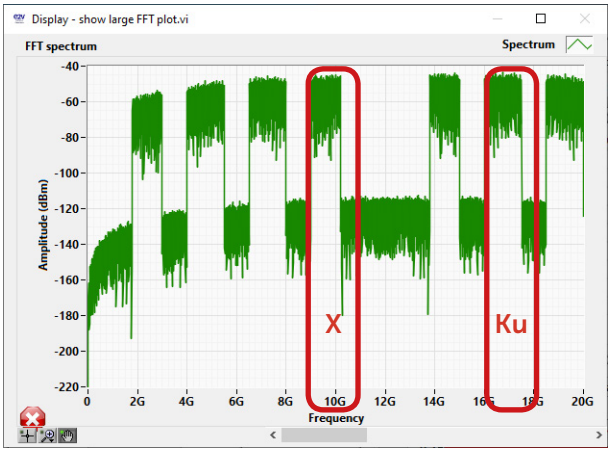

b) X+Ku band in RF mode in the 2nd and 3rd NZs.

Fig. 3 DAC output noise-like spectrum.

The NRZ output of the DAC is low-pass filtered at 5.5 GHz in order to avoid aliasing. Then, it is subsequently amplified and sent to a broadband antenna. The RF output is instead filtered with a bi-band filter to select the X-band in the 2nd NZ and the Ku-band in the 3rd NZ as highlighted in Fig. 3b.

The proposed multi-band SAR architecture shown in Fig. 4 adopts a pulsed radar scheme. Therefore, a circulator is used for each of the two antennas for connecting the receiving chain. Similar to the DAC outputs, the received signals are low-pass filtered for the L+C channel and bi-band filtered for the X+Ku channel before they are amplified and digitised using two ADCs working with the same sampling clock at 12 GHz.

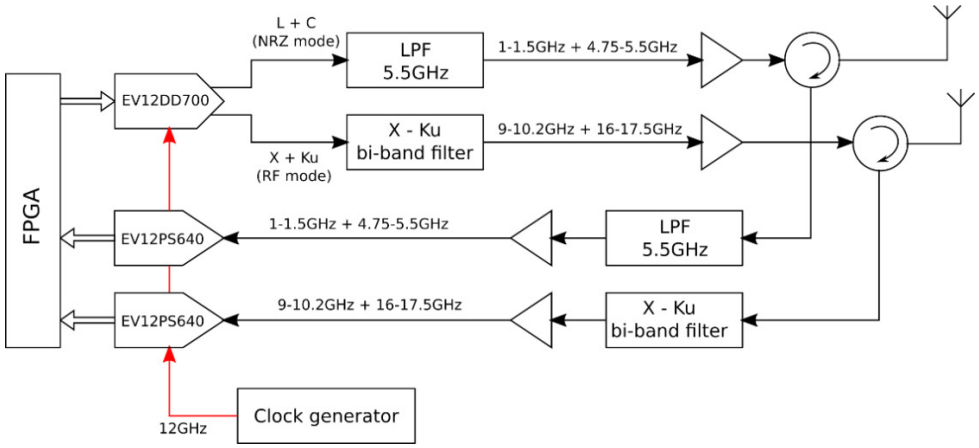

Fig. 4. Multi-band SAR architecture.

Fig. 5 illustrates the frequency planning for the two ADCs. L- and C-bands are directly sampled without aliasing because both fall in the 1st NZ equal to 6 GHz. On the other hand, since the X- and Ku-bands are in the 2nd and 3rd NZs, they fold without overlap in the 1st NZ in the ranges 1.8÷3 GHz and 4÷5.5 GHz, respectively. A high-performance Field Programmable Gate Array (FPGA) implements an arbitrary-waveform generator for the synthesis of the desired radar signals and handles the high-speed digital signals from the ADCs to the high-speed Solid-State Disks (SSD).

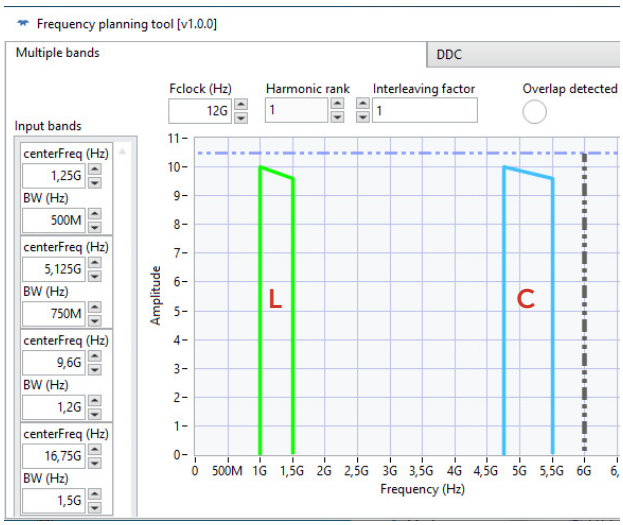

a) L+C band.

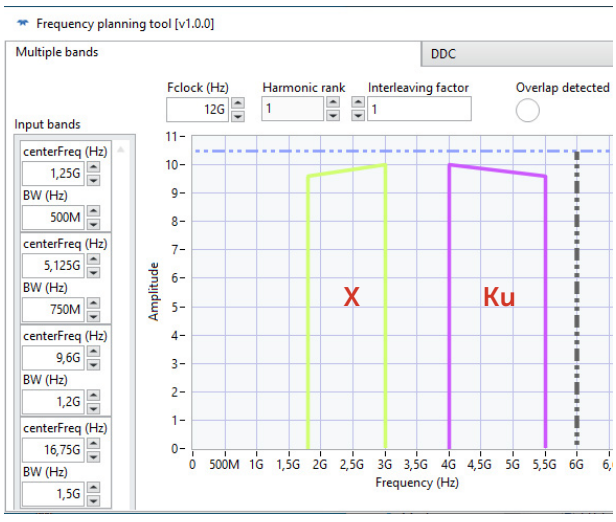

b) X+Ku band.

Fig. 5. ADC frequency planning in the 1st Nyquist Zone.

In the front-end architecture, the input and output filters are of particular importance. The output filters are necessary to select the desired bands and to suppress the unwanted aliased bands. On the other hand, in order to prevent interference from other out-of-band signals and reduce the overall noise level, input filters are necessary to filter out the noise and unwanted signals. These filters can be designed on microstrip technology using multi-band filter techniques. Another option could be to split the broadband signal into two separate bands which will be filtered with single-band filters and then recombined.

Intermediate driver stages will be needed to match the output level of the DACs to the required power levels at the input of the power amplifiers. Power amplifiers should be able to handle adequate power to meet the transmitted power requirements on each frequency band. Since the system is pulse-based, it is necessary to consider the average levels of transmitted power and this simplifies the choice of amplifiers. Wideband circulators, at the outputs of the power amplifiers, are necessary to share the same antenna between transmitters and receivers.

On the receiver side, depending on the transmitted power, the low noise amplifiers (LNA) should be protected by power limiters devices. Otherwise, they could be damaged during the transmission phase due to the poor isolation of the circulators (20 dB typically).

DEVELOPMENT OF AN AIRBORNE SYSTEM DEMONSTRATOR

The use of a single antenna for all the four operating frequency bands may allow a single-phase centre for the formation of the SAR images. However, the ultra-wide frequency-span from 1 GHz to 18 GHz is difficult to be accommodated in a single antenna with a tolerable compromise between gain and antenna size. Also, since the L- and C-bands will be synthesized and digitised with the same DAC and ADC and likewise for the X- and Ku-bands, it is convenient to implement two separate analogue chains as illustrated in Fig. 4.

For an airborne application, the L- and C-bands can be transmitted and received using a broadband horn antenna as the Ainfo LB-560 [6], capable of offering a fairly constant gain of 10-12 dBi across the 0.5÷6 GHz frequency-span as shown in Fig. 6. On the other hand, a multi-octave horn antenna as the Ainfo LB-60180-20 [7] with a 6÷18 GHz bandwidth can handle both the X- and Ku-bands with a gain of about 20 dB at X-band and 22 dBi at Ku-band as plotted in Fig. 7.

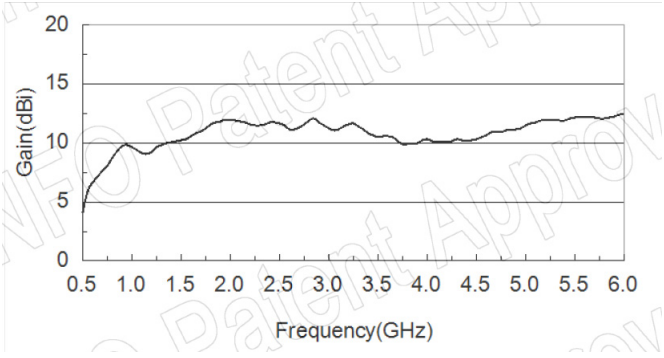

Fig. 6. LB-560 broadband antenna gain

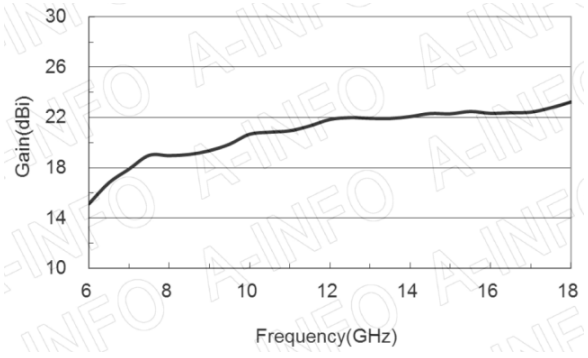

Fig. 7. LB-60180-20 multi-octave antenna gain

In the case of the L+C band, the power amplification can be carried out for instance by the power amplifier RFLUPA0706GG [8] from RF-Lambda which has a typical power output of 48dBm in a frequency range of 0.7÷6 GHz. For example, the RF-Lambda RFLUPA0618GE [9] model might be considered in the X+Ku band. This amplifier has a typical output power of 50 dBm in a frequency range of 6÷18 GHz.

A pass-band harmonic suppression filter might be necessary in output of the power amplifiers. In this case, depending on the transmitted power, microstrip power handling should be carefully evaluated. A possible choice for a high-power wideband circulator in the X+Ku band could be the DORADO International 4CCM14-1 [10] coaxial model that can cover a range of 9÷18 GHz with a power of 150 W. In the case of the L+C band, a circulator with such large fractional bandwidth could be difficult to be found. An alternative could be the use of a high-power coaxial switch as the model RFSP2TR5M06GS by RF-Lambda [11].

In such a high-frequency digital system, a low-jitter clock signal is essential. The clock generator can be implemented using a signal synthesizer based on a phase-locked loop. In this regard, the Analog Devices microwave synthesizer ADF4152, which integrates a voltage-controlled oscillator, provides excellent noise characteristics [12]. The clock distributor can then be realized using high-frequency narrow-band splitters.

The Hitech Global HTG-960 Virtex UltraScale+ VU19P development platform [13] is a good FPGA board candidate which allows for the connection with the DACs and the ADCs using the FPGA Mezzanine Card (FMC) standard. The FMC interface allows also for the connection of Non-Volatile Memory Express (NVMe) high-speed SSD, potentially in Raid0 configuration, for recording the acquired data.

The functionalities of the proposed system could be demonstrated over an ultralight aircraft as the Tecnam P92JS SmartBay [14] which offers the possibility of installation of experimental equipment in a dedicated pod under the wing.

EXPECTED RADAR PERFORMANCE

Assuming the system components proposed so far, the expected SAR performance has been computed with the parameters summarized in Table 1. Conservative values for losses and noise figure have been considered. An aerial platform has been also assumed to fly at a ground speed of 40 m/s and 2000 m above the mean ground level.

Parameter	Symbol	Units	L	C	X	Ku
Central frequency	f_0	GHz	1.25	5.125	9.6	16.75
Transmit power peak	P_t	dBm	45	45	47	47
Signal bandwidth	B_s	MHz	500	750	1200	1500
Repetition frequency	PRF	Hz	2000	8000	10000	12000
Duty cycle	η	%	10	10	10	10
Pulse duration	T_i	μs	50	12.5	10	8.33
Noise figure	F_N	dB	8	8	8	8
Receiver bandwidth	B_r	MHz	600	900	1440	1800
Radio frequency loss	L_{RF}	dB	6	6	6	6
Signal processing loss	L_{DSP}	dB	6	6	6	6
Antenna gain	G_a	dBi	10	12	20	22
Antenna elevation -3dB beamwidth	θ_{el}	deg	47.69	39.40	14.46	9.03
Antenna azimuth -3dB beamwidth	θ_{az}	deg	43.83	47.84	16.18	9.87
Antenna depression angle	Ψ	deg	-35	-35	-45	-45
Slant range resolution (nominal)	dr	cm	30	20	12.5	10
Slant range min (@-3dB antenna)	r_{min}	m	2337	2451	2530	2630
Slant range max (@-3dB antenna)	r_{max}	m	10369	7591	3266	3081
Swath (@-3dB antenna)	Δr	m	8032	5141	736	451
Synthetic aperture length	L_{SAR}	m	2806	3094	804	488
Integration time	CPI	s	84.19	92.82	24.12	14.66

Table 1. Simulation parameters.

With the proposed parameters, the NESZ at the various bands can be computed following (1) derived from [15].

$$NESZ(r) = \frac{(4\pi)^3 r^4 L_{RF} L_{DSP} k_B T_N F_N B_r}{P_t G_a^2 \left(\frac{c}{f_0}\right)^2 \eta T_i B_s PRF 2 r_0 \tan\left(\frac{\theta_{az}}{2}\right)} \quad (1)$$

where k_B is the Boltzmann constant, T_N is the reference temperature of 290°K and r_0 is the slant range at the swath centre. Assuming a distributed reflectivity of 0 dBm²/m², Fig. 8 depicts the received power from the ground patches at the various sub-bands as a function of the slant range. The total integrated power from the whole -3dB footprint of the antenna is also indicated. Since the L- and C-bands share the LB-560 antenna which has a half-power beamwidth larger than 39deg in elevation, the swath at such frequencies is very large ranging from 2337 m to 10369 m at L- band. Despite the LB-560 antenna having almost the same gain at L- and C-bands, the received power at C-band is 20 dB lower than L-band because of the different free-space attenuation. On the other hand, X- and Ku-bands share the LB-60180-20 which is more directive. Therefore, the swath at the two higher bands is narrower.

Fig. 9 shows the expected NESZ as a function of the slant range at the various sub-bands. The expected NESZ is better than -23 dBm²/m² and -25 dBm²/m² at Ku- and X-band, respectively. The footprint of the low-frequency antenna would allow for SAR image formation up to more than 10 km at L-band but with a poor sensitivity. However, since a NESZ better than -20 dBm²/m² represents a value accepted to be a good quality parameter for SAR images, the maximum imaging range for L- and C-bands is limited to 5819 m and 4092 m, respectively.

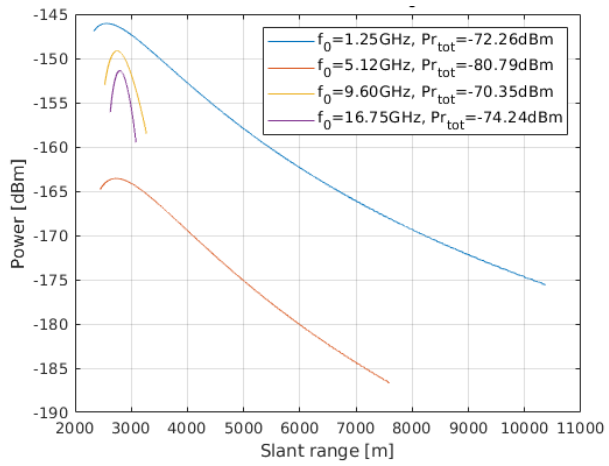

Fig. 8. Received power assuming σ⁰ = 0dBm²/m².

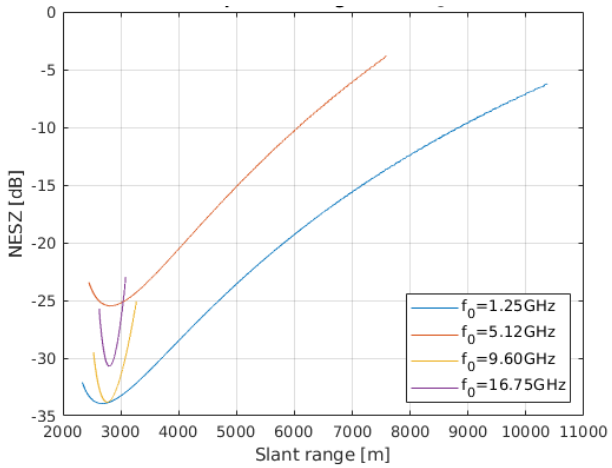

Fig. 9. NESZ.

ON-BOARD PROCESSING AND EXPECTED DATA RATES

In order to reduce the data rate of the data to be recorded, the received signal at the four bands is sampled and pre-processed on-board according to the scheme depicted in Fig. 10. In particular, each sampled band is Digital-Down Converted (DDC) to the baseband according to the respective central frequency in the 1st NZ. Then, the sample rate is decimated by means of a Cascaded Integrator-Comb (CIC) filter in order to accommodate the instantaneous bandwidth. A Finite-Impulse Response (FIR) filter is used to compensate for the CIC filter response. The filtered signals are then range-compressed by means of cross-correlators (Xcorr) and limited at the range bins of interest for each band with a range over-sampling factor of four. The aggregated data-rate of 6160 MB/s is finally sent to a two channels Raid0 Gen.4 NVMe IP [16] which writes the range-compressed data on two Gen.4 NVMe SSDs at about 3080MB/s each [17].

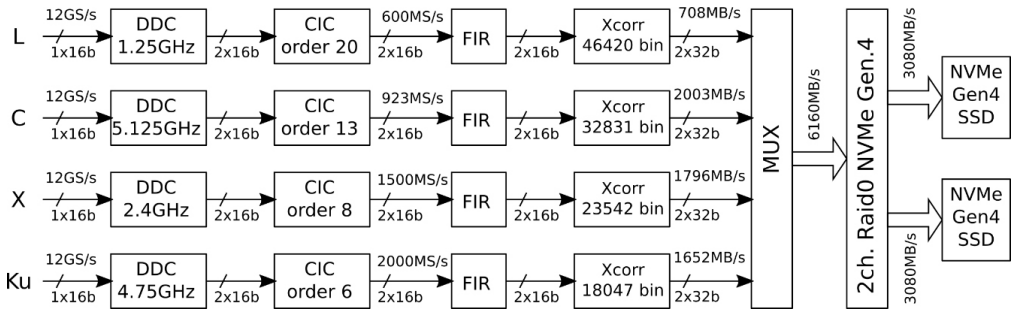

Fig. 10. On-board processing architecture.

CONCLUSION AND PERSPECTIVES

In this paper, a feasibility study of a fully-digital multi-band SAR system operating at L-, C-, X- and Ku-bands has been introduced. First of all, a description of the key enabling technologies consisting of innovative DAC and ADC from Teledyne e2v has been done. Then, a preliminary architecture of the proposed pulse-based SAR system has been described. Finally, examples of commercial components and technologies have been described to assess the feasibility of an airborne system demonstrator capable of multi-band SAR image formation from an aerial platform. Expected performance in terms of NESZ, received power and data rates have been derived and analysed.

Future perspective could involve a detailed analysis of the system performance in terms also of the impulse response, phase linearity and spurious levels, and then the development of the proposed airborne multi-band SAR demonstrator. Such a demonstrator might be a first step of a wider technology roadmap bringing an updated design and then a development of a spaceborne payload pushed by the new space-race of agencies and private companies.

REFERENCES

[1] *Flores, Africa & Herndon, K. & Thapa, Rajesh & Cherrington, Emil.; "The SAR Handbook: Comprehensive Methodologies for Forest Monitoring and Biomass Estimation", 2019.*
[2] *Davis, Mark Edward; "Foliage penetration radar"; SciTech Pub., 2011.*
[3] *Skolnik, M. I. «Radar Handbook 3Rd Edition/Merill I. Skolnik», 2008.*
[4] *www.semiconductors.teledyneimaging.com/en/products/digital-to-analog-converters/ev12dd700/ (co-funded by Interstellar EU project, from Horizon 2020 Space programme under grant agreement N° 730165)*
[5] *www.semiconductors.teledyneimaging.com/en/newsroom/how-to-sample-x-through-ka-band-rf-to-support-sdr-systems/*
[6] *www.ainfoinc.com.cn/en/pro_pdf/new_products/antenna/Broadband%20Horn%20Antenna/tr_LB-560.pdf*
[7] *www.ainfoinc.com.cn/en/pro_pdf/new_products/antenna/Broadband%20Horn%20Antenna/tr_LB-60180-20.pdf*
[8] *www.rflambda.com/pdf/poweramplifier/RFLUPA0706GG.pdf*
[9] *www.rflambda.com/pdf/poweramplifier/RFLUPA0618GE.pdf*
[10] *www.dorado-intl.com/wp-content/uploads/2017/05/4CCM14-1.pdf*
[11] *www.rflambda.com/pdf/switchers/RFSP2TR5M06GS.pdf*
[12] *www.analog.com/en/products/adf4372.html#product-overview*
[13] *www.hitechglobal.com/Boards/VirtexUltraScale+_VU19P_Board.htm*
[14] *www.tecnam.ro/avioane/p92-js-smartbay.html*
[15] *Doerry, Armin. "Performance Limits for Synthetic Aperture Radar - second edition", 2006.*
[16] *www.dgway.com/products/IP/NVMe-IP/dg_nvmeg4ip_raid0x2_refdesign_xilinx_en.pdf*
[17] *www.samsung.com/it/memory-storage/nvme-ssd/980-pro-2tb-nvme-pcie-gen-4-mz-v8p2t0bw/*

For further information, please contact:

Daniele Staglianò,
Chief Executive Officer,
daniele.stagliano@echoes-tech.it

Nicolas Chantier,
Marketing Director
Signal and Data Processing Solutions
nicolas.chantier@teledyne.com